UNIVERSITÀ DEGLI STUDI DI PADOVA

Dipartimento di Fisica e Astronomia "Galileo Galilei"

Corso di Laurea in Fisica

Tesi di Laurea

In beam gamma spectroscopy with a ^{84}Zr beam: comparison of data with a Monte Carlo simulation

Relatore

Dr. Francesco Recchia

Correlatore

Dr. Jeongsu Ha

Laureando

Andrea Pompermaier

Anno Accademico 2020/2021

Abstract

The study of the nuclear structure of exotic nuclei, which lie very far from the stability valley, is fundamental to test many physical theories. It requires the use of nuclear reactions induced by fast radioactive beams and use-of-the-art detectors, such as the γ-ray tracking array GRETINA.
This thesis reports part of the results of an experiment performed at the National Superconducting Cyclotron Laboratory (NSCL) at Michigan State University (MSU) during the summer 2020.
The main purpose of this work is the numerical simulation of the experimental process to completely reproduce the interaction of an exotic nuclear beam of ^{84}Zr with a ^{9}Be target. All the physical information about the reaction process are extrapolated through comparisons between the experimental data and Monte Carlo simulations, performed with GEANT4. This platform, which contains the experimental geometry and the detectors information, can reproduce the entire interaction mechanism, from the incoming beam distribution in space and momentum to the Doppler corrected γ-ray spectrum. The analysis consists in finding the optimal parameters necessary to correctly reproduce experimental data. The results of this work are used to analyze other more exotic reaction channels where statistics is scarce. The final goal of this experiment is the measurement of the lifetime of the first excited state in ^{84}Mo.

Contents

Introduction

Nuclei are complex systems composed of protons and neutrons, also called *nucleons*, which form the basis of known matter. Their properties depend on collective nucleons interactions which define the shape and the energy states of a nucleus. There are many models that try to describe nucleons interactions to explain and make predictions about nuclear structure, such as the shell model. Theoretical assumptions can be proved from experimental results, such as measurements of energy and lifetime of excited states, thus providing fundamental insights on the in-medium nucleon-nucleon interaction. Exotic nuclei, with their high unbalance between the number of protons (Z) and neutrons (N), turn out to be perfect candidates to test nuclear models in extreme conditions.
Nuclei with N = Z show interesting nuclear structure properties since protons and neutrons occupy the same valence orbitals and peculiar proton-neutron correlations can be investigated [1]. Many information can be obtained from systematic studies of excitation energies and reduced transition probabilities. A systematic study of the excitation energy of the first 2^+ state and its lifetime has been a major effort of the international nuclear physics community. Such study faces more and more experimental difficulties when heavier N = Z nuclei are studied. Recently $^{80}_{40}$Zr 2^+ state could be measured [2]. $^{84}_{42}$Mo, another even-even exotic nucleus with N = Z, is naturally the next step. An important test bench for the theoretical models is the reduced quadrupole transition probability, $B(E2)$, which is directly connected to the quadrupole deformation of the nucleus. This parameter is obtained from the experimental estimation of the lifetime of the first 2^+ excited state by the analysis of γ-ray spectrum exploiting Doppler shift technique properly.
This work focuses on high statistics reaction channels ^{84}Zr and ^{82}Zr from which derive important information about secondary beam selection and reaction products identification. The final results will be directly applied to ^{84}Mo. It is indeed of fundamental importance to have under control the kinematics of the reaction and to have an accurate quantitative description in terms of Monte Carlo simulation.
Exotic nuclei have been produced at NSCL by in-flight projectile fragmentation through high energy collisions starting from stable beams accelerated to relativistic energies against a ^{9}Be target. From the interaction of the secondary beam with a beryllium fixed target the first excited states are populated. These unstable states decay emitting γ-rays that are detected by an High-Purity Germanium (HPGe) γ-ray tracking array called GRETINA. Picosecond-range lifetime of excited states is measured using Doppler shift methods such as the recoil distance method (RDM) [3]. Some relevant details about the experimental setup are described in Chapter 1, from beam production techniques until HPGe γ-ray detectors and S800 spectrograph.
Numerical simulations are employed to reproduce complex reactions with several unknown parameters. The process which describes the interaction of the beam with a fixed target, for example a knockout reaction, depends on several dynamic variables such as the momentum, kinetic energy and velocity of incoming and outgoing beam, but there are also other parameters that are related to the experimental setup that have to be properly set, such as target density and target position respect to the detectors. The whole process can be reproduced using particular simulation programs. GEANT4 is a platform based on C++ which is used for Monte Carlo simulations of particles interaction with matter in a particular experimental setup. Through GEANT4 packages it has been possible to reproduce beam profile and γ-ray spectrum of each reaction channel. Afterwards the simulations are compared with data using the minimum χ^2 method in order to extrapolate the best fit parameters that are necessary to reconstruct the whole process. In Chapter 2 some of the analysis techniques used for this work are

summarized. Eventually, using the optimal reaction parameters, the complete γ-ray spectra of ^{84}Zr and ^{82}Zr have been simulated and then compared with the experimental ones (Chapter 3).

Chapter 1

Experimental Details

The NSCL has been one of the pivotal facilities in experimental nuclear physics. The facility produces fast radioactive beams, so high resolution techniques and multiple devices are necessary to produce, transport and identify them. The purpose of this chapter is to briefly illustrate the instruments used during this specific experiment performed at NSCL.

1.1 NSCL Beam Production

The whole process starts from the Superconducting Source for Ions (SuSI) that is an Electron Cyclotron Resonance (ECR) source used in this case to produce a beam of $^{92}Mo^{+}$ ions. Using the K500 superconductive cyclotron the primary beam is accelerated and directed to a second cyclotron K1200 [4]. The names of cyclotrons derive from the "K-number" corresponding to the maximum energy to which a proton beam can be accelerated. At this point primary beam has typically an energy of $\sim 140 MeV/u$. Exotic nuclei are produced using the technique of *projectile fragmentation*: the primary beam is directed against a ^{9}Be production target located before A1900 separator. Targets are usually made in beryllium due to its physical properties such as high number density, high melting point, and good thermal conductivity. After the interaction of ^{92}Mo with the target a fraction of the incoming beam fragments into different isotopes among which there are ^{86}Mo and ^{84}Zr. A1900 separator is composed of four superconducting 45° dipole magnets and 24 superconducting quadrupole focusing magnets that select secondary beams produced after the fragmentation [5].

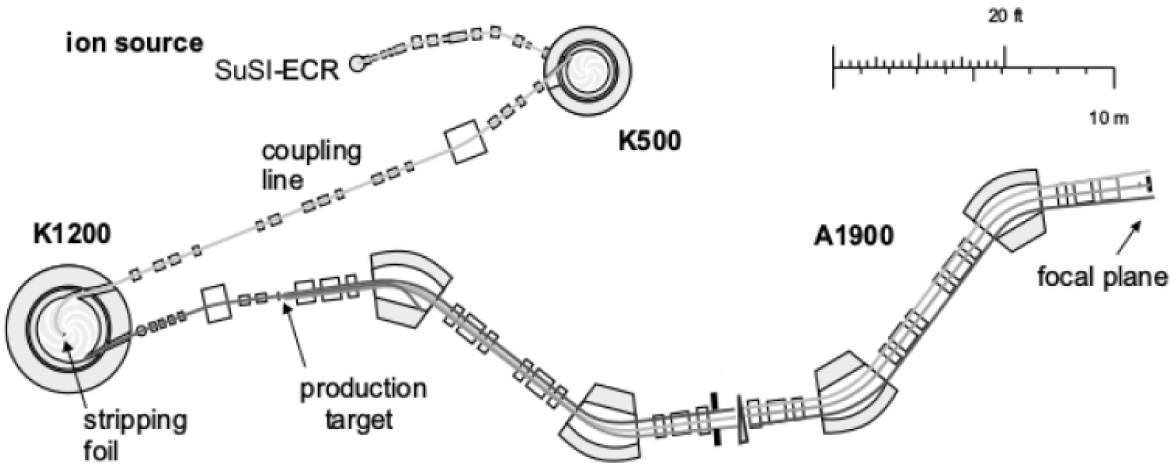

Figure 1.1: Figurative representation of experimental equipment used to produce rare isotopes at NSCL. Taken from [6].

In order to separate different nuclides by mass and nuclear charge, a combined technique based on magnet-rigidity analysis and energy-loss in degrader materials is used starting in A1900 and concluding in S800 spectrograph [7]. The first step to purify secondary beams consists in dipole magnets. A particle of mass m, velocity v and charge q has a bending radius ρ in a magnetic field B given by the formula [4]:

$$B\rho = \frac{mv\gamma}{q} = \frac{Am_u c}{Ze}\beta\gamma \tag{1.1}$$

(where m_u is the unified atomic mass, e the elementary charge and A and Z are the mass and atomic number respectively)
The slits are used to select specific isotopes by blocking unwanted ions. Once the secondary beam is purified enough, at the end of A1900, the beam impinges on a second ^{9}Be target where specific reactions occur, for example, ^{84}Mo from ^{86}Mo or ^{82}Zr from ^{84}Zr (two-neutron knockout reactions). The γ-rays produced through the reaction are detected by GRETINA. The recoiling nuclei are identified by the S800 spectrograph [8].

1.2 GRETINA HPGe Array Detector

GRETINA (*Gamma-Ray Energy Tracking In-beam Nuclear Array*) is the HPGe array detector featured γ-ray tracking. It is composed of twelve modules with four detectors placed on a ring at $\theta = 58°$ with respect to the beam-line and the other eight in a second ring at $\theta = 90°$. For this experiment the target was positioned 20 cm upstream of the center of GRETINA. Currently GRETINA covers a detection solid angle of $\sim 2\pi$ but it is planned to increase the apparatus with other 15 modules to a 4π array that will be called GRETA (*Gamma Ray Energy Tracking Array*) [9]. γ-ray tracking is possible thanks to the segmentation of each module that is divided into 36 segments (Fig. 1.2): the interaction of γ radiation with HPGe detectors induces an electric signal for every single segment. Using specific analysis algorithms it is thus possible to reconstruct γ-ray's path, with a resolution better than few millimeters, and its energy: this procedure is called *γ-ray tracking*.
Technological constrains limit the size of the detectors used to detect γ radiation. As a consequence in a real detector it is possible that some photons exit from the detection region without having deposited completely their energy. This type of process is typically due to multiple Compton scatterings which increase the spectrum background. Most of events, however, are low-multiplicity Compton scatterings that lose entirely their energy in the detectors. Generally, a single photon interacts with different crystals before stopping. These subsequent interactions can be simulated by GRETINA's algorithm in γ-ray tracking through the following relation:

$$E_{\gamma'} = \frac{E_\gamma}{1 + \frac{E_\gamma}{m_e c^2}(1 - cos\theta)} \tag{1.2}$$

(where $E_{\gamma'}$ is the scattered energy and E_γ the initial energy of the photon, m_e is the electron mass and θ is the scattering angle of photon)
The Klein-Nishina formula is employed to calculate the differential cross section of the γ-electron interaction [10]:

$$\frac{d\sigma}{d\Omega} = Zr_e^2 \left[\frac{1}{1 + (h\nu/m_e c^2)(1 - cos\theta)}\right] \times \left[1 + \frac{(h\nu/m_e c^2)^2(1 - cos\theta)^2}{(1 + cos^2\theta)[1 + (h\nu/m_e c^2)(1 - cos\theta)]}\right] \tag{1.3}$$

(where r_e is the radius of the electron and ν is the photon's frequency)
The algorithm matches single interaction points and calculates the total probability of that path starting from Eq. 1.3 and using as θ the angle between two subsequent points. From all possible Compton scatterings it is selected the most probable. In this way it is possible to calculate the correct energy of every single photon and the first interaction point. These parameters play an important rule in Doppler correction.

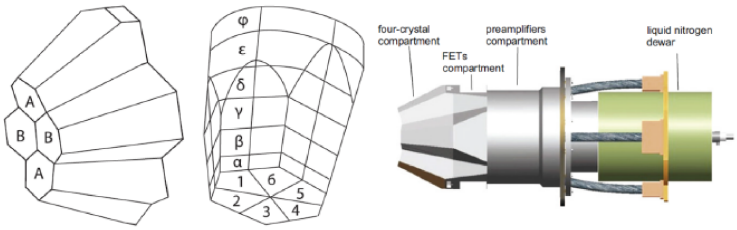

Figure 1.2: Illustration of GRETINA's module. In the middle picture it is illustrated crystals segmentation, on the left the hexagonal arrangement for grouping crystals into a quad and on the right an overall view of a module. Taken from [11].

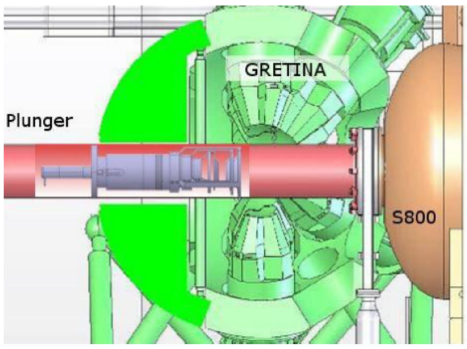

Figure 1.3: Layout of the experiment apparatus. Taken from [12].

1.2.1 γ-ray Doppler Correction

In these type of experiments relativistic beams are used for high energy collisions and reactions with target. Beam velocity varies in the range of $0.3 - 0.4c$ so de-excited nuclei γ-ray spectrum has a considerable Doppler shift. The following formula connects the γ-ray energies measured in the two frames:

$$E_{rest} = E_{lab}\frac{(1 - \beta cos\theta)}{\sqrt{1 - \beta^2}} \tag{1.4}$$

(where E_{rest} and E_{lab} are respectively the γ-energies measured in rest frame and laboratory systems) From γ-ray tracking GRETINA estimates the first interaction point of a photon in the detector and then it calculates the emission angle θ respect to the target position (Fig. 1.4). Using the Eq. 1.4 the energy measured by detectors can be corrected and then it is possible to get the γ-ray energy emitted in the nucleus rest frame system through event-by-event Doppler-correction algorithms. This procedure uses the approximation of considering the emission at the target position, that is a good assumption only for very short lifetimes (some picoseconds). For longer lifetimes indeed the difference from the real emission angle θ' is not negligible. The result is that the angle used in Doppler correction is biased and thus (from Eq. 1.4) the energy estimated results to be lower than the real one. This effect is evident in the spectrum analysis (see also Sections 3.3.1 and 3.3.2) because long lifetime transition peaks present long low-energy tails. The Fig. 1.5 shows the simulated response of GRETINA on the same $2^+ \rightarrow 0^+$ transition using three different lifetimes. The significant difference of the spectra demonstrates that the peak shape itself can be exploited for estimating the lifetime of the state.

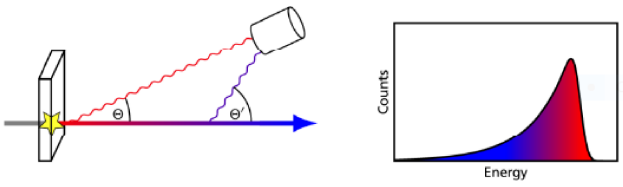

Figure 1.4: An illustration of Doppler effects on γ-ray spectrum. Longer lifetimes increase the discrepancy between the angle θ calculated with respect to the target and the real emission angle θ': for long lifetimes the peak shape becomes asymmetric. Taken from [13].

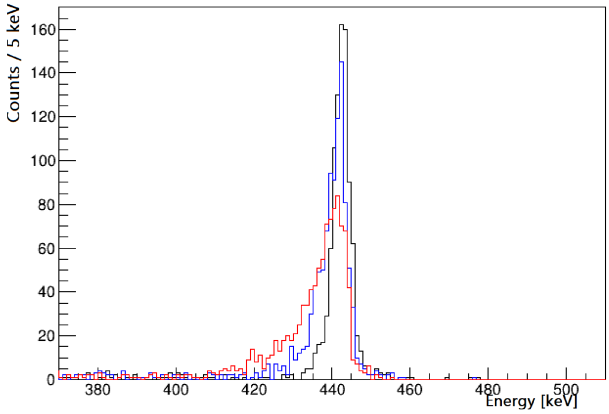

Figure 1.5: Simulation of $2^+ \rightarrow 0^+$ for the target-only case of ^{84}Mo using different lifetimes: 20 ps (Black), 50 ps (Blue) and 100 ps (Red).

1.3 Plunger Setup

A technique to measure lifetimes in the range of 1 ps to 1000 ps is the *Recoil Distance Method* (RDM) based on the plunger setup [3]. *Plunger* experimental setup consists of a target and one or two degraders, which are foils used to decrease the beam velocity (in this experiment it has been used only one). In Fig. 1.9 there is an illustration of a plunger device called TRIPLEX, very similar to that used in this experiment except for a second degrader generally used to estimate longer lifetimes. Since the energy measured in the laboratory system depends on beam velocity, the Doppler corrected spectrum has a double peak shape: the energy detected by nuclei that decay after the degrader is lower than nuclei which decay between target and degrader, so their peak appear shifted on the left low-energy side. With this setup it is possible to estimate the fraction of nuclei that decay before or after the degrader by their spectral peaks amplitude, from which it can be estimated the excited state lifetime.

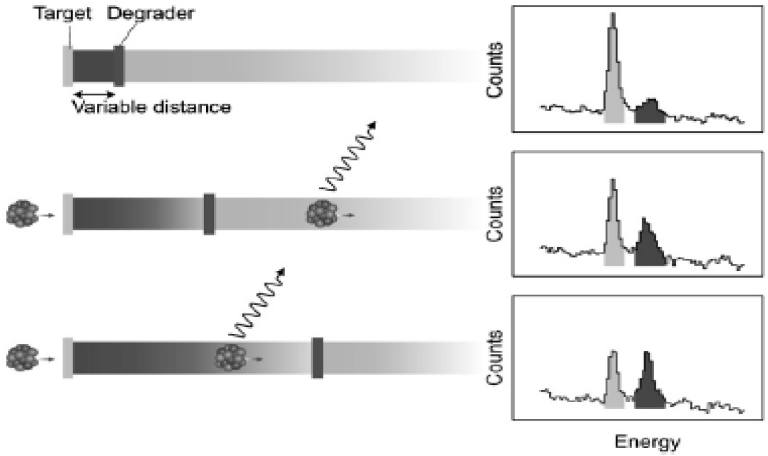

Figure 1.6: Schematic representation of Doppler corrected spectra in a plunger setup using different target-degrader distances. Taken from [3].

The remarking feature of plunger is shown through two types of simulations in Fig. 1.7 and 1.8 comparing the two peaks in Doppler corrected spectrum. In Fig. 1.7 there are three simulations obtained by changing target-degrader distance: increasing this distance also the second peak increases since there are more decays before the degrader. In Fig. 1.8 instead it is compared the same spectrum but changing the only lifetime: with longer lifetimes there are more decays after degrader and so the first peak increases.

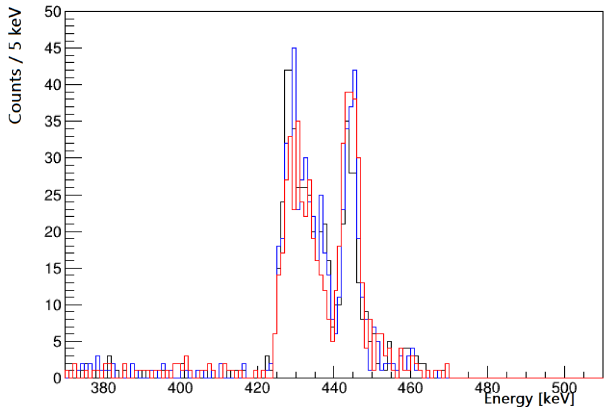

Figure 1.7: Simulation of $2^+ \rightarrow 0^+$ for ^{84}Mo plunger setup using different target-degrader distances with a fixed lifetime of 35 ps: 1 mm (Black), 1.5 mm (Blue) and 2.0 mm (Red).

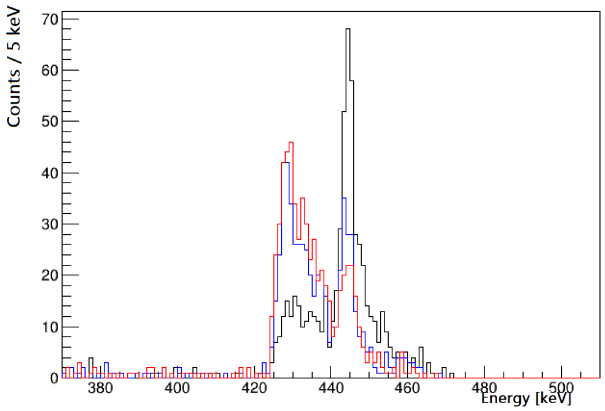

Figure 1.8: Simulation of $2^+ \rightarrow 0^+$ for ^{84}Mo plunger setup using different lifetimes with a fixed target-degrader distance of 1 mm: 10 ps (Black), 35 ps (Blue) and 50 ps (Red).

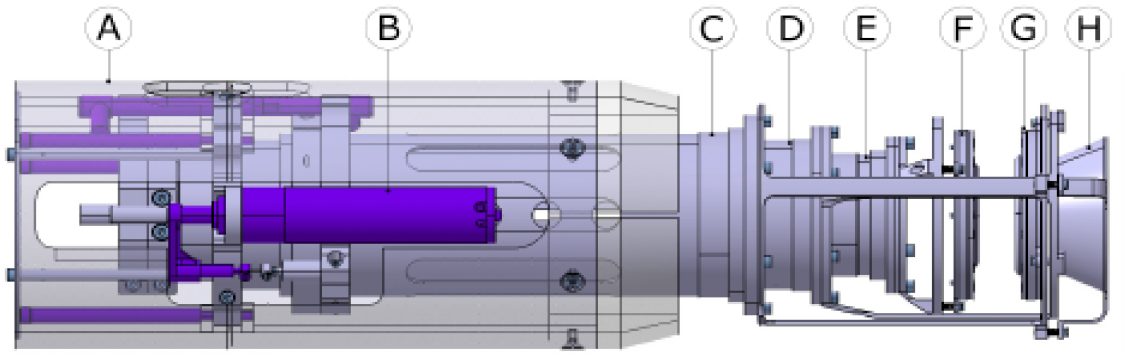

Figure 1.9: Schematic of plunger device. It is composed of: outer casing (A), piezoelectric motors to move target (B), external (C) and internal (D) cylinder structures connected respectively to the first and second degrader (this is a general TRIPLEX plunger setup made of 2 degraders, although in this experiment it has been used only one), first (E) and second degraders (G) and the target (F). In this figure primary beam comes from the left side. Taken from [14].

1.4 S800 Spectrograph

Downstream the A1900 separator there is S800, which is an high resolution, large acceptance magnetic spectrometer used to identify secondary beams in order to select different reaction products [8]. It is divided in two parts: the first is the S800 *Analysis Line*, while the second is S800 *Spectrograph*. The Analysis Line is upstream the target and it is used to identify secondary beams before reaction. This is possible through *Extended Focal Plane* (XFP) and *Object* scintillators with high timing resolution necessary for time-of-flight (ToF) measurements [15]. Immediately after the second target there is the S800 spectrograph (Fig. 1.10) which is a PID device composed by:

- Superconducting dipole magnets that focus the outgoing ions in the non-dispersive (y) and dispersive (x) planes in order to increase the acceptance of the spectrograph.
- Two position-sensitive detectors *Cathode-Readout-Drift-Counters* (CRDC) which measure (X,Y) positions of particles which pass through them (Fig. 1.11): from the incoming (X1,Y1) and outgoing (X2,Y2) positions they can also provide angular distributions (a_{fp} and b_{fp}). Charged beams that pass through this tracker ionize a gas contained inside the detector. (X,Y) positions are deduced from the distribution of induced charges on the cathode by measuring the drift time of electrons [16].
- A ionization chamber is positioned downstream of the two CRDC trackers. The gas inside it is a mixture of 90% Ar and 10% CH_4. When charged particles enter in the ion chamber they lose by ionization their energy. Using an uniform electric field electrons drift towards anode where, from the amplitude of the induced signal, it is possible to reconstruct the total energy loss. It can be also used for identifying different reaction products (with different velocity v and charge q) by their stopping power (Eq. 1.5) [17]

$$-\frac{dE}{dx} = \frac{4\pi q^2 e^4}{m_e v^2} NZ \left[ln \frac{2m_e v^2}{I(1-\beta^2)} - \beta^2 \right] \tag{1.5}$$

  (N and Z are respectively the number density and atomic number of the material, e the elementary charge and I the ionization energy of the material)
- Three scintillators (E1, E2, E3 in Fig. 1.10) follow the ion chamber. When a particle traverses them they emit a light signal which can be amplified by PhotoMultiplier Tubes (PMT). E1 scintillator is used as trigger for Data Aquisition (DAQ) system and combining its information with the other scintillators (E2, E3 and *Object*) the ToF of a particle through the spectrograph

can be calculated: this value is important to estimate the mass and charge of the nuclei. The principle of the ToF-$B\rho$ technique is based on the laws of motion. An ion with charge q and momentum p passing through a beam line with a total flight path of length L, a fixed magnetic rigidity $B\rho$, time-of-flight given by T, has a nuclear mass m related to these variables by [18]:

$$m = p \cdot \sqrt{\left(\frac{T}{L}\right)^2 - \frac{1}{c^2}} \overset{1.1}{=} qB\rho \cdot \sqrt{\left(\frac{T}{L}\right)^2 - \frac{1}{c^2}} \tag{1.6}$$

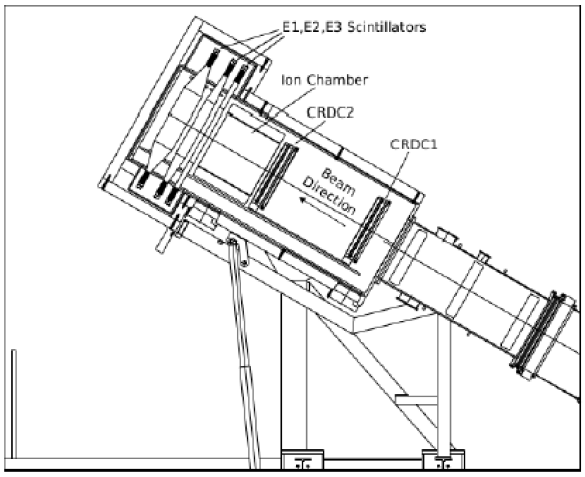

Figure 1.10: Schematic of S800 spectrograph focal plane. Taken from [19].

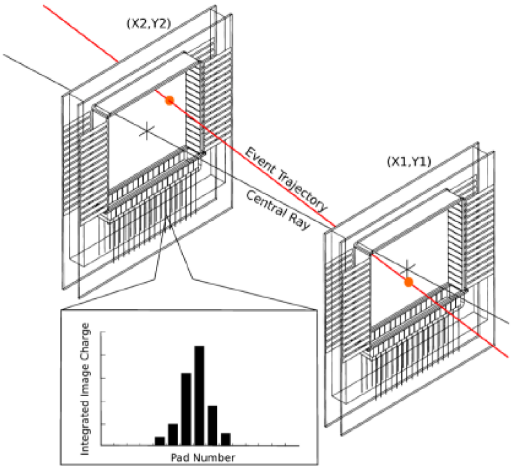

Figure 1.11: Schematic of CRDC detectors. Taken from [20].

1.4.1 Particle Trajectory Reconstruction

The individual particle trajectory can be reconstructed through S800 information. There are some necessary parameters used to describe the interaction with target: the position at the target (denoted by the coordinates x_{ta} and y_{ta}), the corresponding dispersive and non-dispersive angles a_{ta}/b_{ta} and the relative kinetic energy spread $\frac{dT}{T} = d_{ta}$ (where ta indicates that they are referred to the target). The CRDCs in S800 spectrograph measure x_{fp}, y_{fp}, a_{fp} and b_{fp} respect to the focal plane (fp). Then it is possible to calculate target reaction parameters using the inverse map S^{-1}:

$$\begin{bmatrix} a_{ta} \\ b_{ta} \\ y_{ta} \\ d_{ta} \end{bmatrix} = S^{-1} \begin{bmatrix} x_{fp} \\ a_{fp} \\ y_{fp} \\ b_{fp} \end{bmatrix} \tag{1.7}$$

In Eq. 1.7 the dispersive position at the target (x_{ta}) doesn't appear because it is assumed to be a delta function centered to zero (with further analysis it is observed that there is a small shift on the dispersive direction which can be corrected). Moreover d_{ta} distribution is estimated using S800 ToF and energy loss information, but also position and angular distributions.
The inverse map is produced with experimental geometry and known physical parameters such as $B\rho$, mass and charge of the particles to reproduce the whole process properly. $B\rho$ (Eq. 1.1) is an experimental parameter that is tuned in order to select particular reaction channels (in the case of unreacted beam without target it was set $B\rho = 3.0651Tm$ so that the ^{86}Mo incoming beam trajectory coincided with S800 focal plane center) and it is useful, along with other beam information like the mass m and the electric charge q, to obtain the incoming and outgoing beam energy through the simulation program $LISE^{++}$, which simulates the fragmentation process occurred in S800 to separate radioactive beams [21]. The inverse map allows an event-by-event analysis which returns the experimental distributions (d_{ta}, y_{ta}, a_{ta} and b_{ta}) necessary for the simulations. Recoiling beam parameters affect also Doppler corrected spectra changing significantly the resolution: their optimization becomes necessary to correctly reproduce the final spectra (Section 3.3).

Chapter 2

Analysis Techniques

Complex phenomena, with several unknown parameters, can be studied using Monte Carlo simulations. This computational method consists in an algorithm which produces an arbitrary set of random numbers, that follow a certain probability distribution, with the purpose of reproducing a particular physical process. In this work all known experimental processes, from beam interaction with target to γ-ray detection, have been modelled through appropriate distributions which depend on some characteristic variables. The goal consists in finding the optimal parameters that allow to produce simulations which faithfully reproduce the experimental data. In this chapter, it will be introduced the simulation program GEANT4 used during the analysis and the set of parameters that have to be subsequentially optimized to arrive, at the final step, to the γ-ray spectrum simulation.

2.1 GEANT4 Monte Carlo Simulation

GEANT4 is a simulation framework based on C++ programming language which is widely used in Nuclear and Subnuclear physics to reproduce beam interaction with matter [22]. In particular, for this analysis, it has been used the *G4Lifetime* package, which contains NSCL's experimental geometry around the secondary target focal plane, including ^{9}Be target and detectors frame. Macros used for this work contain different types of information about:

- **incoming and outgoing beam**: the simulation code can replicate beam profile using different parameters such as momentum distribution, incoming and outgoing kinetic energy, angular and position distributions. It can also replicate different types of reaction with the target, for example knockout reactions or Coulomb scatterings.
- **target**: $250 mg/cm^2$-thick ^{9}Be target, with a thickness of $1.325 mm$, is positioned $204.6 mm$ upstream of the GRETINA center. Using simulation packages it is possible to adjust this value to improve experimental agreement. Usually the outgoing beam energy or other parameters used in GEANT4 simulations are calculated using $LISE^{++}$, however this program has stopping power tables slightly different. Little discrepancies from the ideal case can heavily affect the results: for this reason it has been introduced a parameter called scale-density (sd) which is used to correct these small deviations between the two programs.
- **analysis**: there are some information about GRETINA's detectors that are necessary to reproduce γ-ray spectrum. Firstly it is important to properly select which detectors were used during the experiment, since detection position affects Doppler corrected spectrum lineshape (Section 1.2.1). Simulation code is capable to reproduce γ-ray tracking uncertainties which affect GRETINA's resolution and also Doppler corrected spectrum from β, momentum, angular and position distributions of decaying particles. It is also possible to replicate the presence of slits that limit S800 acceptance blocking part of the beam.
- **spectrum**: γ-ray transitions can be replicated using all optimal parameters previously obtained and adding in the macro file the information about γ decays.

Typically an experimental distribution contains from 2000 to 100000 events, however in the simulation it is possible to set an arbitrary number of events: in high statistic simulations statistical uncertainties become negligible respect to the experimental ones. Generally a good statistic simulation is formed by more than 100000 events. GEANT4 produces a ROOT file which contains all necessary simulated distributions such as: angular and position distributions $a_{ta}/b_{ta}/d_{ta}/y_{ta}$ (defined in Section 1.4.1), Doppler add-back spectrum, background and single detector spectra.

2.2 G4Lifetime Parameters Optimization

The procedure of parameters optimization requires several steps that have to be done sequentially. The final goal is to reproduce the correct simulated spectrum from which it is possible to estimate the lifetime of the transitions. In general, some parameters can be directly obtained from experimental data with simple calculations, such as the incoming/outgoing velocities, and others that require complex analysis since they affect more than one experimental distribution simultaneously: in this case a multi-parametric optimization is necessary.
The optimal simulation parameters, determined through the comparison with experimental data distributions, are obtained using χ^2-minimization procedure. There are two kind of runs that can be analyzed, the *reacted* and *unreacted*: these channels differ in the selection range. The reacted case undergoes a more significant loss of energy, due to the interaction with the target, respect to the unreacted one: this means that after the dipole magnets of S800 the two types of outgoing beams are split and they can be analyzed separately. The optimization procedure can vary from case to case (depending, for example, on the shape of distribution or on the statistics) but there are some common steps that have to be made to fix some parameters and thus to reduce the degrees of freedom. The method used for the analysis is the following:

1. $B\rho$ value and experimental deviation from the central trajectory can be used to calculate the outgoing beam velocity through $LISE^{++}$ program. The outgoing beam velocity and momentum distribution of unreacted without target case coincide with the incoming ones that can be set for the next simulations.

2. $LISE^{++}$ simulation returns also the outgoing beam energy KE_{out} that can be fixed in order to optimize scale-density (sd). This parameter depends on KE_{out} and momentum distribution (d_{ta}): typically this correction is in the range [0.95, 1.05]. Varying sd in a small range near 1 and comparing simulations with experimental d_{ta} (for the unreacted with target case) it can be optimized and kept as constant for further analysis.

3. The next step involves creating a simulation which replicates the reaction with target mechanism. There are three fundamental parameters which characterize the energy transferred within the reaction target:

   - $dp_{frac} = \frac{p_{out}}{p_{in}}$ (where p_{in} and p_{out} are respectively the incoming and outgoing longitudinal momentum);
   - dp is the centroid of transversal momentum distribution;
   - dp_{FWHM} is the *Full Width at Half Maximum* of transversal momentum distribution.

   All these parameters affect at the same time a_{ta}, b_{ta}, d_{ta} and y_{ta} distributions.

4. Once all parameters have been optimized it is possible to obtain a γ-ray spectrum simulation. This procedure, which is described in detail in Section 3.3, requires the relative intensities, energies and lifetimes of each nuclear transition: these values can be calculated from the experimental spectra, the efficiency curve and the literature.

Chapter 3

GEANT4 Simulation Results

In this chapter the most relevant results, derived from the analysis of experimental data applying the procedure described in Chapter 2, are presented with some details about the different methods used. The optimization procedure often leads to qualitative results. The parameters uncertainties are often difficult to be carefully estimated because the software modelization of the process is only schematic. The quality of the final spectra demonstrates the validity of the approach. In this type of analysis it is necessary to compare the results with experimental data constantly and to verify that they are physically acceptable: sometimes the numerical methods used to find optimal values can produce wrong results that can be corrected by making other physical assumptions.

3.1 Target Scale-density

The outgoing beam energy of ^{84}Zr unreacted without target, obtained from $B\rho$ in $LISE^{++}$ simulation, is $KE_{in} = 98.82\ AMeV$: since there is no target it coincides with the incoming beam energy. The outgoing beam energy for unreacted with target ^{84}Zr, instead, is $KE_{out} = 66.8\ AMeV$.
Firstly it has been implemented the incoming beam momentum distribution using d_{ta} experimental data of ^{84}Zr unreacted without target (Fig. 3.1).

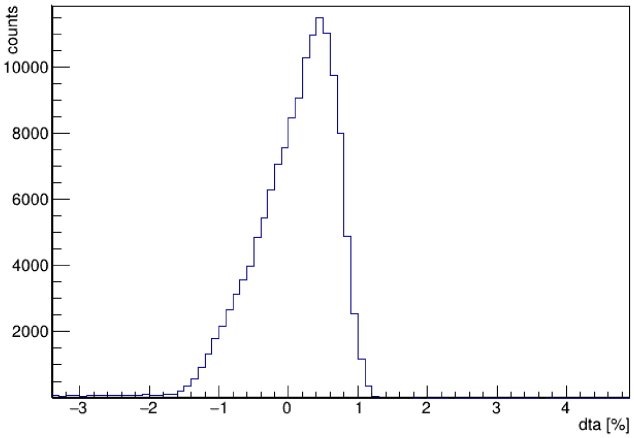

Figure 3.1: ^{84}Zr unreacted without target experimental d_{ta} distribution. It has been used to simulate incoming ^{84}Zr beam momentum distribution.

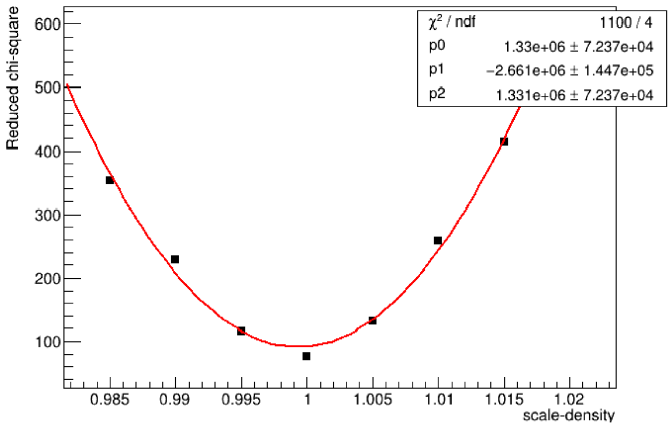

Figure 3.2: Reduced χ^2 for scale-density optimization in the range [0.985, 1.015]. The minimum is for scale-density = 1.

The reaction parameters dp and dp_{FWHM} have been set to 0, instead $dp_{frac} = 1$: the unreacted with target case is the reference for the reacted ones. It has been made a scan varying scale-density in the range of [0.985, 1.015]. From d_{ta} unreacted with target data and the simulation comparison it has been obtained the χ^2 distribution which can be fitted using a second order polynomial (Fig. 3.2).

The comparison range selected is [-3%, 3 %]: this is the range used to renormalize different distributions for the comparison with experimental data in Fig. 3.3 and 3.4. The optimal scale-density is:

$$sd = 1.000 \pm 0.005$$

This uncertainty has been approximately estimated by the distributions comparison in Fig. 3.3: the uncertainty estimation is very difficult because it requires to know every single possible experimental error, so in this case it is preferable to use a wider range.
Experimental data distributions are obtained through inverse map applied to S800 information. It happens very often that there is some noise in data (especially in d_{ta}): the top of experimental d_{ta} seems cut and on the right side there are a lot of fluctuations due to other reaction channels contaminants.

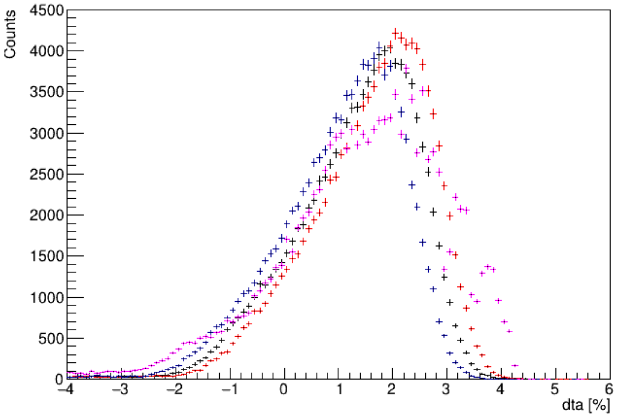

Figure 3.3: Comparison of ^{84}Zr d_{ta} unreacted with target experimental distribution (purple) with different scale-density simulations: 0.995 (red), 1.000 (black) and 1.005 (blue).

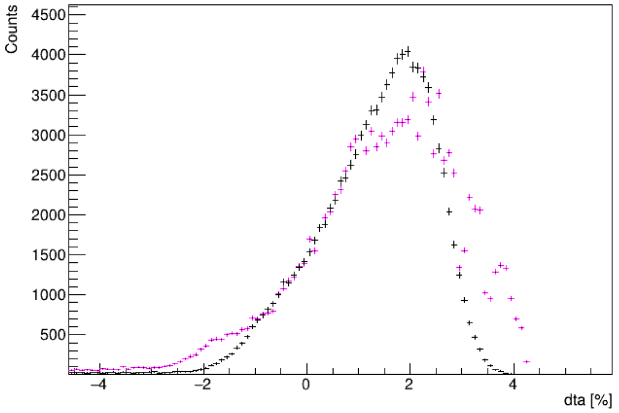

Figure 3.4: Comparison of optimized 1.000 scale-density (black) and data (purple). The right side of experimental distribution is made of other reaction channel contaminants.

3.2 Reaction Parameters

There are three parameters which have to be optimized before simulating the total spectrum: dp_{frac}, dp and dp_{FWHM}. These are called *reaction parameters* since they describe the interaction process occurred at the target. They affect together d_{ta}, a_{ta}, b_{ta} and y_{ta} distributions which must be properly set to reproduce Doppler corrected spectrum.
Firstly the optimal dp_{frac} can be derived from d_{ta} and then, taking it as fixed, the other two parameters can be optimized simultaneously using d_{ta} and b_{ta} distributions and varying dp and dp_{FWHM}.
In this work they have been considered only d_{ta}, b_{ta} and y_{ta} because to correctly reproduce a_{ta} distribution are necessary further analysis: the dispersive angular distribution, which is equal to the non-dispersive one (b_{ta}) in the simulation, in reality it is a bit wider. y_{ta} can be optimized varying the non dispersive distribution width DY by using minimum χ^2 procedure.

3.2.1 ^{9}Be(^{84}Zr, X)^{84}Zr

The incoming beam of ^{84}Zr has a kinetic energy of $KE_{in} = 98.82\ AMeV$, obtained from the unreacted without target case. The outgoing beam reacted with target of ^{84}Zr has a kinetic energy, derived from $LISE^{++}$ simulation, of $KE_{out} = 63.8\ AMeV$.

dp_{frac} optimization

The energy loss in the reaction process $d_{ta} = \frac{dT}{T}$ depends on $dp_{frac} = \frac{p_{out}}{p_{in}}$: changing dp_{frac} the d_{ta} distribution shifts. A useful method that can be used to optimize this parameter consists in varying dp_{frac} until simulated d_{ta} centroid coincides with the experimental one (see Section 3.2.3). In case of ^{84}Zr, however, d_{ta} experimental distribution is limited at 4% by a slit and the centroid is not in the

selected range. In this case it is convenient to compare by eyes different simulated d_{ta} distributions with experimental data changing dp_{frac} in the range of [0.990, 1.000]. A first comparison (Fig. 3.5) shows that until $dp_{frac} = 0.995$ the distribution has a peak before the slit. The range for dp_{frac} is limited into [0.995, 0.999] so, using an other comparison (Fig. 3.5) with $dp_{frac} = 0.995$(red) - 0.997(black) - 0.999(blue), the optimal value is:

$$dp_{frac} = 0.997 \pm 0.002$$

The width of d_{ta} distribution can be modified by using different dp and dp_{FWHM} (in this case $dp = dp_{FWHM} = 400MeV$) however the lineshape comparison is a good way to get information about dp_{frac}. Obviously this method has uncertainties that are difficult to be estimated: surely the optimal dp_{frac} is in the range of [0.995, 0.999]. As a first step it can be assumed $dp_{frac} = 0.997$ and then, after the optimization of the other parameters, it can be verified if it is a correct assumption. Anyway the uncertainty used for this parameter considers all possible cases contained within the range [0.995, 0.999].

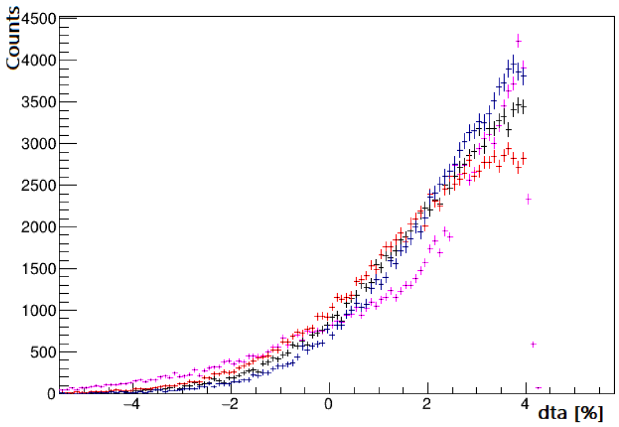

Figure 3.5: Comparison of ^{84}Zr d_{ta} reacted with target experimental distribution (purple) with different dp_{frac} simulations: 0.993 (red), 0.995 (black) and 0.997 (blue).

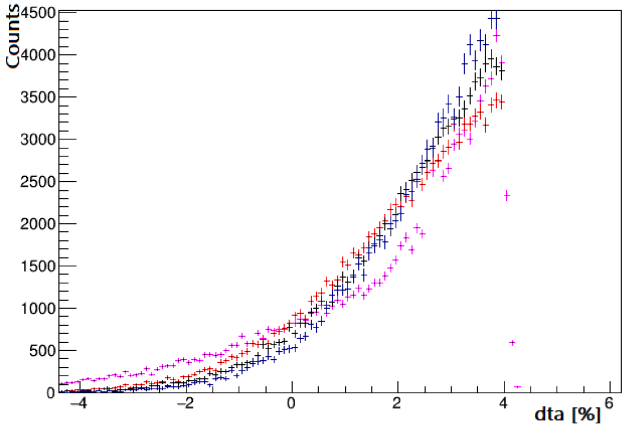

Figure 3.6: Comparison of ^{84}Zr d_{ta} reacted with target experimental distribution (purple) with different dp_{frac} simulations: 0.995 (red), 0.997 (black) and 0.999 (blue).

dp and dp_{FWHM} optimization

dp and dp_{FWHM} have to be optimized simultaneously comparing d_{ta} and b_{ta} distributions with the simulations. It has been scanned dp in the range [300 MeV, 550 MeV] and dp_{FWHM} in the range [550 MeV, 1100 MeV] (with step-size 50 MeV).
Because we need to find a compromise between the two simultaneous optimizations for each simulation it has been calculated the total χ^2 summing the singular χ^2 obtained from the comparison of d_{ta} and b_{ta} with the corresponding experimental distributions. The comparison ranges selected for this scope are:

- d_{ta}: [-6%, 4%]
- b_{ta}: [-40 mrad, 40 mrad]

The total χ^2 in Fig. 3.7 and 3.8 shows a minimum region for dp in the range [350 MeV, 450 MeV] and dp_{FWHM} in the range [750 MeV , 1050 MeV].

To choose the best one it's convenient a direct comparison between a small number of candidates. In this case they have been considered sections of the total χ^2 for dp in the range of [375 MeV, 450 MeV] (with step-size 25 MeV) (the results are presented in Fig. 3.9, 3.10, 3.11 and 3.12). Each section has been fitted with a second order polynomial to get the minimum (since there are big uncertainties the minimum has been approximated to the nearest simulation).

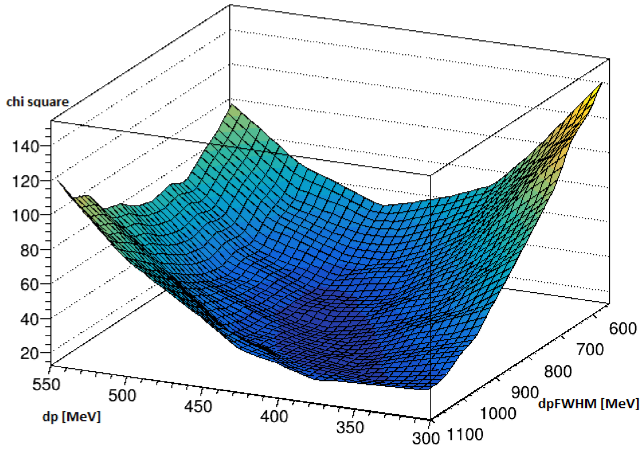

Figure 3.7: 3D view of the total χ^2 for ^{84}Zr obtained from dp and dp_{FWHM} scan.

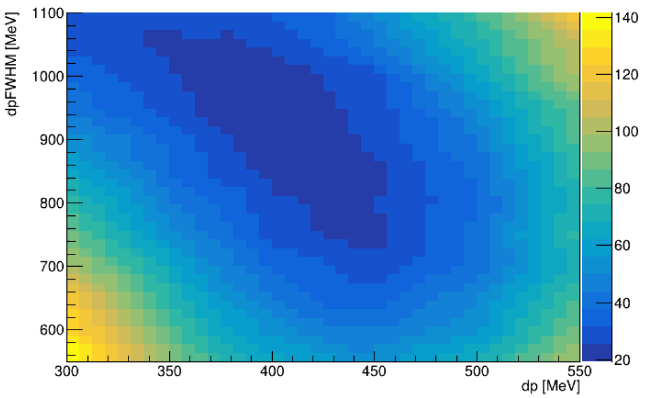

Figure 3.8: 2D view of the total χ^2 for ^{84}Zr obtained from dp and dp_{FWHM} scan.

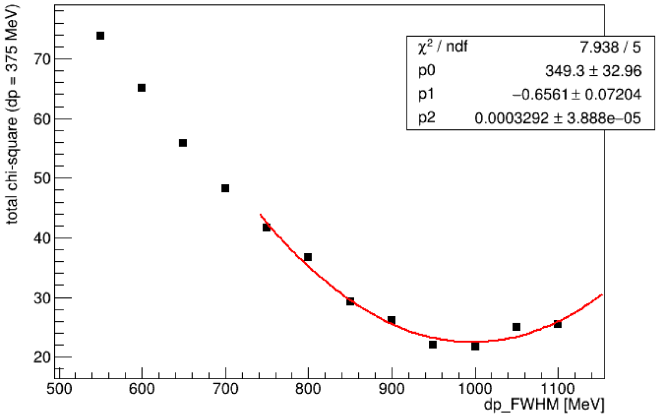

Figure 3.9: ^{84}Zr χ^2 section for $dp = 375MeV$. The minimum is $dp_{FWHM} = 1000$ MeV.

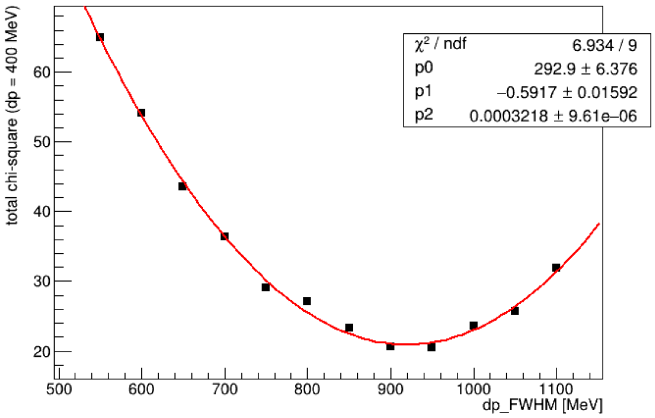

Figure 3.10: ^{84}Zr χ^2 section for $dp = 400MeV$. The minimum is $dp_{FWHM} = 900$ MeV.

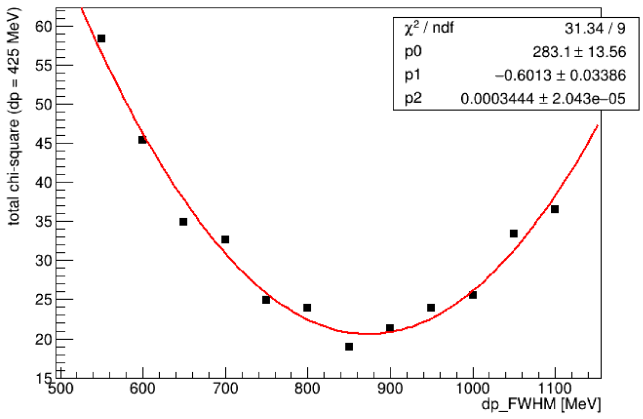

Figure 3.11: ^{84}Zr χ^2 section for $dp = 425MeV$. The minimum is $dp_{FWHM} = 850$ MeV.

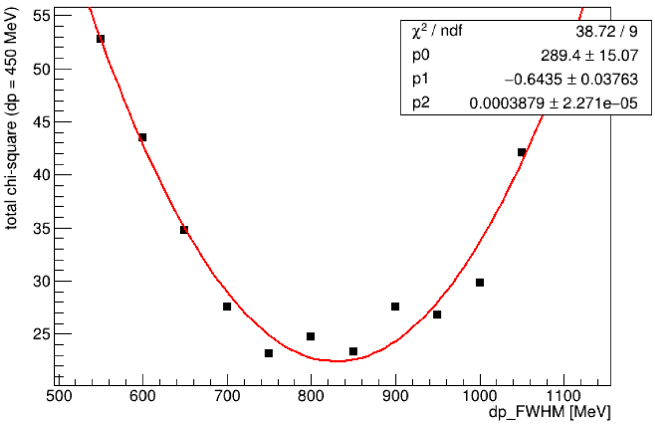

Figure 3.12: ^{84}Zr section for χ^2 $dp = 450MeV$. The minimum is $dp_{FWHM} = 850$ MeV.

From a direct comparison the best simulation, that reproduces at the same time experimental d_{ta} and b_{ta}, has the following optimal values (Fig. 3.13 for b_{ta} and 3.14 for d_{ta}):

$$dp = 425MeV \qquad dp_{FWHM} = 850MeV$$

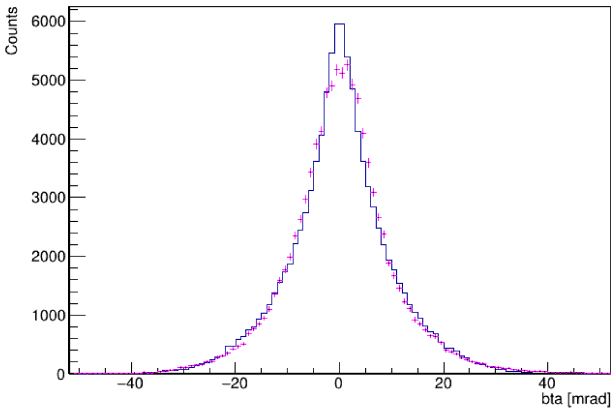

Figure 3.13: b_{ta} distribution of ^{84}Zr optimized with dp = 425 MeV and dp_{FWHM} = 850 MeV: comparison between simulation (blue) and data (purple).

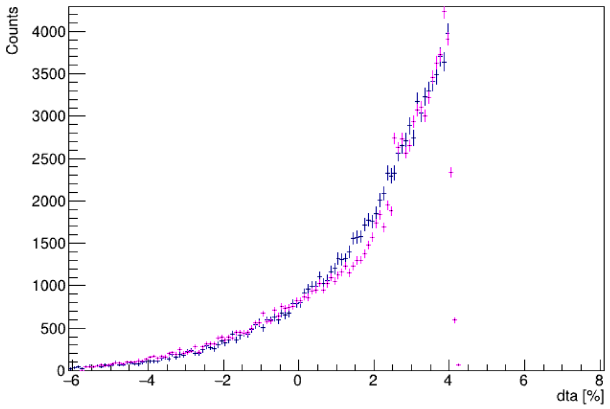

Figure 3.14: d_{ta} distribution of ^{84}Zr optimized with dp = 425 MeV and dp_{FWHM} = 850 MeV: comparison between simulation (blue) and data (purple).

As mentioned before the minimum χ^2 is not well defined, so in practice it's more convenient a direct comparison on a few number of candidates. In reality it occurs very often that, since simulations cannot reproduce exactly the experimental results due to the incompleteness of the underlying model, there are different optimal parameters for b_{ta} and d_{ta}. In this case the two optimal parameters are similar (for b_{ta} is $dp = 450MeV$ and $dp_{FWHM} = 850MeV$, instead in case of d_{ta} is $dp = 375MeV$ and $dp_{FWHM} = 1000MeV$): this is the reason why the total χ^2 bottom is so wide and it is difficult to estimate the uncertainties of the optimal values.

y_{ta} distribution

The non dispersive y_{ta} position distribution depends on two parameters:

- **centroid of distribution**: it can be deduced from experimental data. In this case it is 0.9 mm.
- **DY**: This parameter corresponds to the width of y_{ta} distribution. After fixing the centroid it is the only free parameter and it can be optimized with the minimum χ^2 procedure.

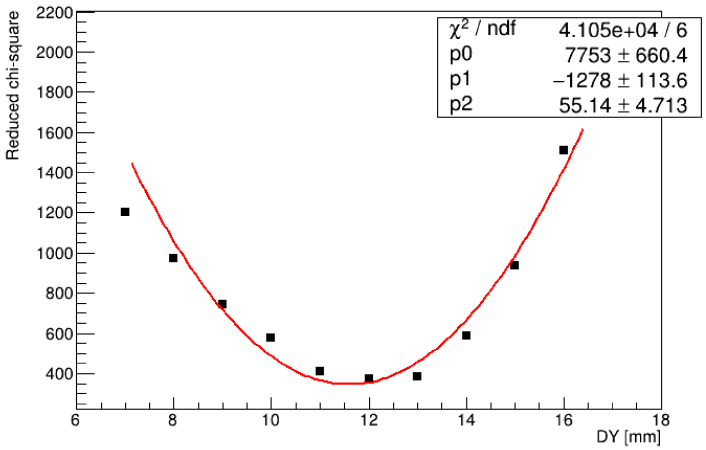

Figure 3.15: χ^2 of ^{84}Zr y_{ta} distribution for DY optimization.

Simulation cannot exactly reproduce experimental y_{ta}, which is asymmetric with a longer tail on the left side, so it has been used as comparison range [-5 mm, 5 mm]. The optimal width is:

$$DY = (12 \pm 1)mm$$

The uncertainty has been estimated from the comparison in Fig. 3.16.

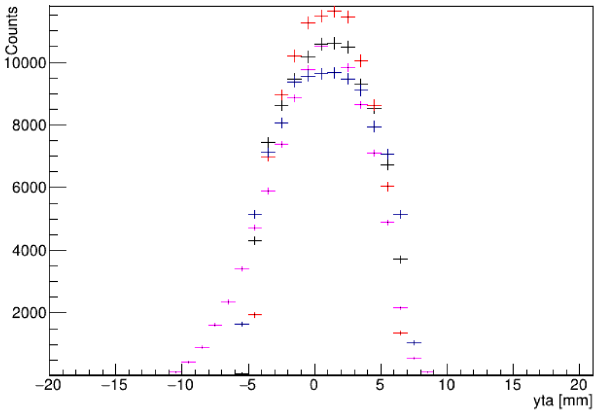

Figure 3.16: Comparison of ^{84}Zr y_{ta} reacted with target experimental distribution (purple) with different DY simulations: 11 mm (red), 12 mm (black) and 13 mm (blue).

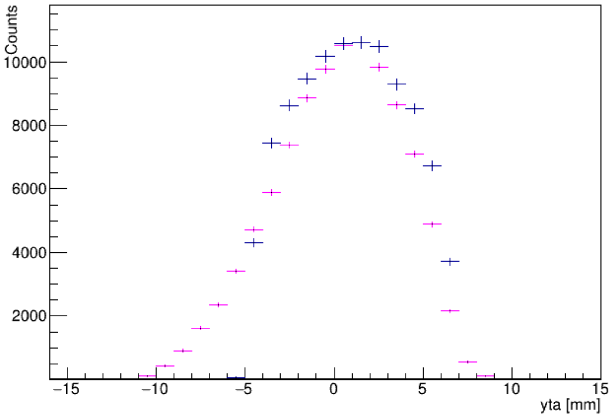

Figure 3.17: ^{84}Zr optimized y_{ta}: $DY = 12$ mm; simulation (blue) and data (purple). The simulation is not capable to completely reproduce the experimental distribution.

3.2.2 ^{9}Be(^{84}Zr, X)^{82}Zr

This reaction channel consists in the fraction of ^{84}Zr primary beam which reacts with the target through a two-neutron knockout reaction to produce ^{82}Zr. The outgoing beam of ^{82}Zr has a kinetic energy of $KE_{out} = 66.8\ AMeV$.

dp_{frac} optimization

In this case it is possible to estimate the optimal dp_{frac} calibrating the centroid position of d_{ta} distribution. First of all experimental d_{ta} has been fitted to a gaussian function to get the centroid position (Fig. 3.18):

$$centroid = (-0.33 \pm 0.02)\%$$

The same procedure has been applied to all d_{ta} simulated distributions with fixed $dp = dp_{FWHM} = 400 MeV$ (this value is an arbitrary choice) and variable dp_{frac} in the range [0.990, 1.000]. In this range there is a linear relation between d_{ta} centroid and dp_{frac} (Fig. 3.19).

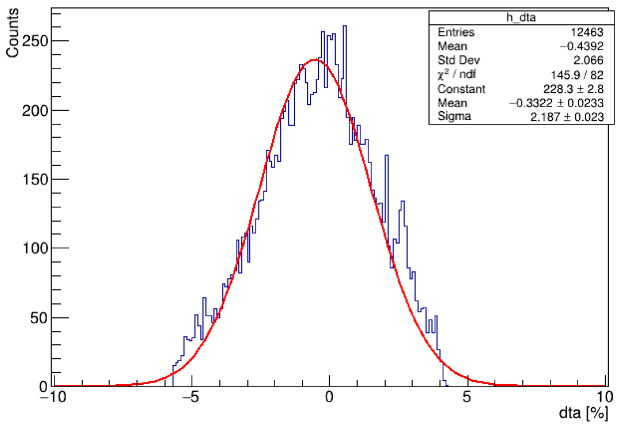

Figure 3.18: Gaussian fit to estimate ^{82}Zr d_{ta} centroid position.

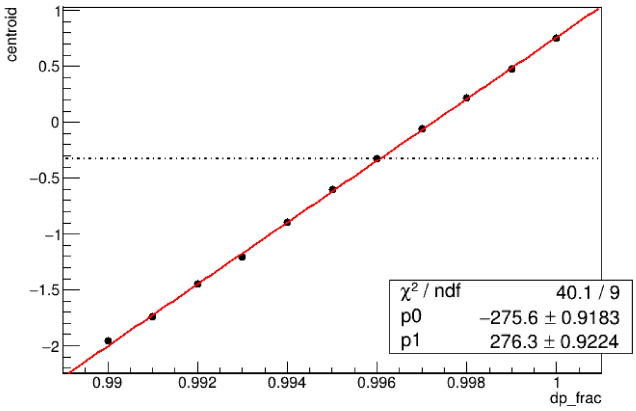

Figure 3.19: d_{ta} centroid vs. dp_{frac} linear fit. The optimized value is $dp_{frac} = 0.996$.

From a linear fit derives the optimal dp_{frac}:

$$dp_{frac} = 0.996 \pm 0.005$$

d_{ta} distribution in reality is not a gaussian. It has been used for the fit only to have an estimation of the centroid position although it involves a large uncertainty.

dp and dp_{FWHM} optimization

Through a procedure similar to that used in the previous case, *dp* has been scanned in the range [250 MeV, 550 MeV] and dp_{FWHM} in the range [250 MeV, 1100 MeV] (with step-size 50 MeV).
For each simulation it has been calculated the total χ^2 of d_{ta} and b_{ta} distributions. The comparison ranges used are:

- d_{ta}: [-6%, 4%]
- b_{ta}: [-40 mrad, 40 mrad]

In Fig. 3.20 and 3.21 is shown the total χ^2 obtained from the *dp* and dp_{FWHM} scan. This function has a minimum for $dp \in [375MeV, 450MeV]$ and $dp_{FWHM} \in [500MeV, 900MeV]$.

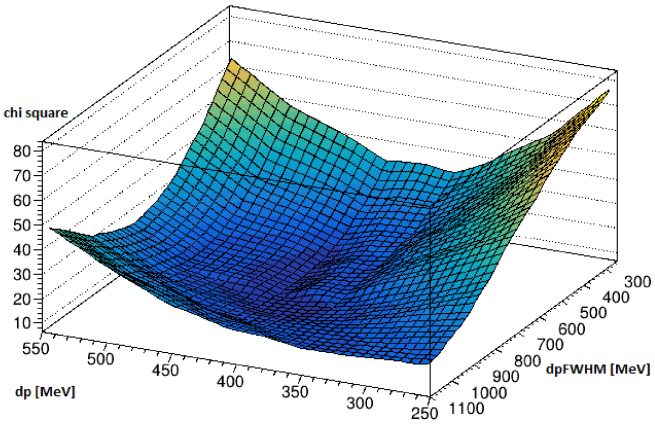

Figure 3.20: 3D view of the total χ^2 for ^{82}Zr obtained from *dp* and dp_{FWHM} scan.

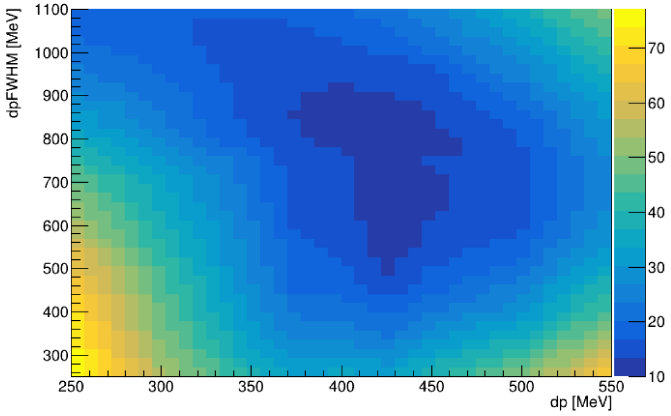

Figure 3.21: 2D view of the total χ^2 for ^{82}Zr obtained from *dp* and dp_{FWHM} scan.

To choose the best one it's convenient a direct comparison between a small number of candidates. The comparison has been made between *dp*-sections of the total χ^2 in the range of [375 MeV, 450 MeV] (with step-size 25 MeV) (The results are presented in Fig. 3.22, 3.23, 3.24 and 3.25).

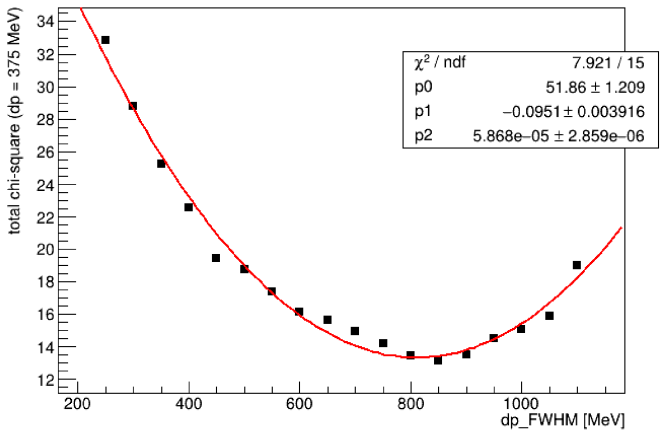

Figure 3.22: ^{82}Zr χ^2 section for $dp = 375MeV$. The minimum is $dp_{FWHM} = 850$ MeV.

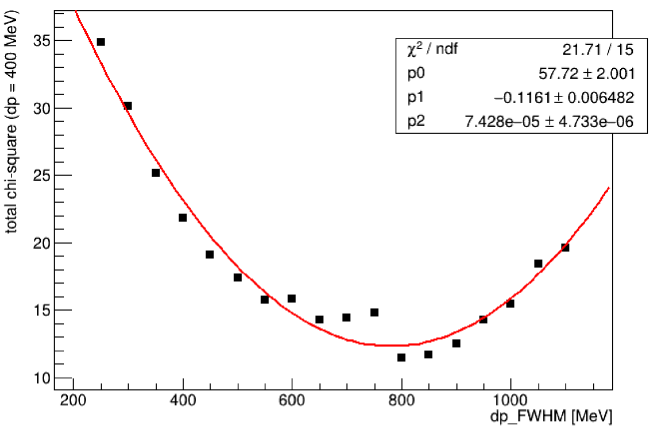

Figure 3.23: ^{82}Zr χ^2 section for $dp = 400MeV$. The minimum is $dp_{FWHM} = 800$ MeV.

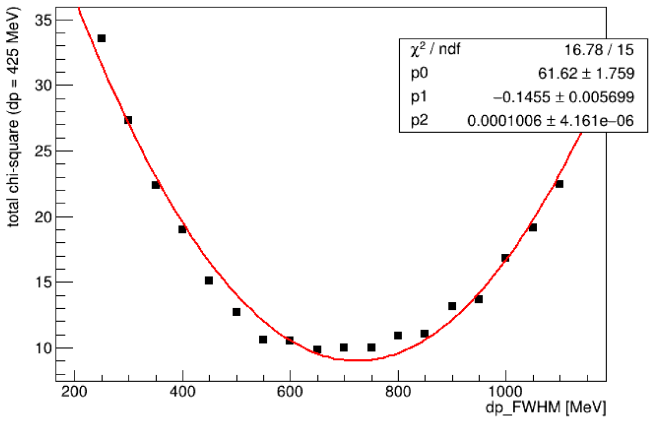

Figure 3.24: ^{82}Zr χ^2 section for $dp = 425MeV$. The minimum is $dp_{FWHM} = 700$ MeV.

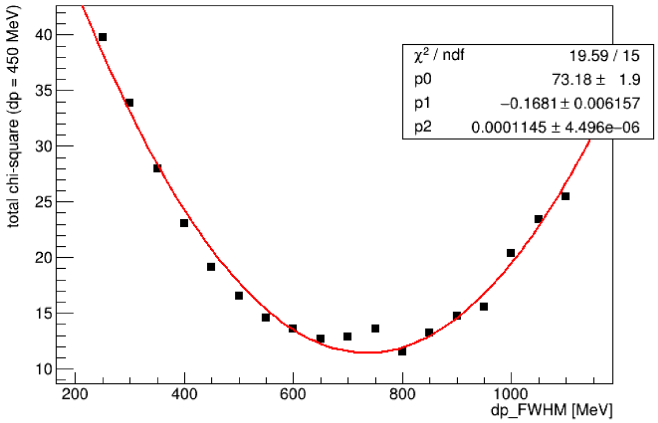

Figure 3.25: ^{82}Zr χ^2 section for $dp = 450MeV$. The minimum is $dp_{FWHM} = 750$ MeV.

The best simulation, that reproduces at the same time experimental d_{ta} and b_{ta}, has the following optimal values (Fig. 3.26 for b_{ta} and 3.27 for d_{ta}):

$$dp = 400MeV \qquad dp_{FWHM} = 800MeV$$

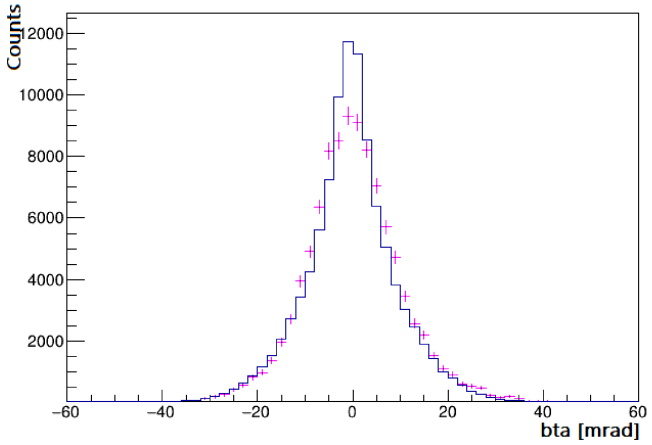

Figure 3.26: b_{ta} distribution of ^{82}Zr optimized with $dp = 400$ MeV and $dp_{FWHM} = 800$ MeV: comparison between simulation (blue) and data (purple).

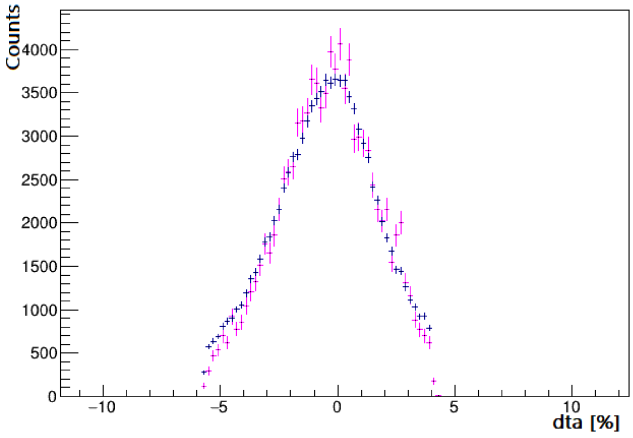

Figure 3.27: d_{ta} distribution of ^{82}Zr optimized with $dp = 400$ MeV and $dp_{FWHM} = 800$ MeV: comparison between simulation (blue) and data (purple).

As in the previous case the optimal parameters for b_{ta} and d_{ta} optimization are a bit different. The final result was obtained by a comparison of the single cases.

y_{ta} distribution

- **centroid of distribution**: In this case it is fixed to zero.
- **DY**: From the minimum χ^2 optimization procedure (performed in the range [-5 mm, 5 mm]) the optimal parameter turns out to be:

$$DY = (12 \pm 1)mm$$

Although from the χ^2 the optimal DY seems to be 13 mm, from the comparison in Fig. 3.29 the best one is $DY = 12$ mm. This method is not precise since the simulated distribution is different from the real case, however it is useful for a qualitative optimization, necessary for spectrum simulation.

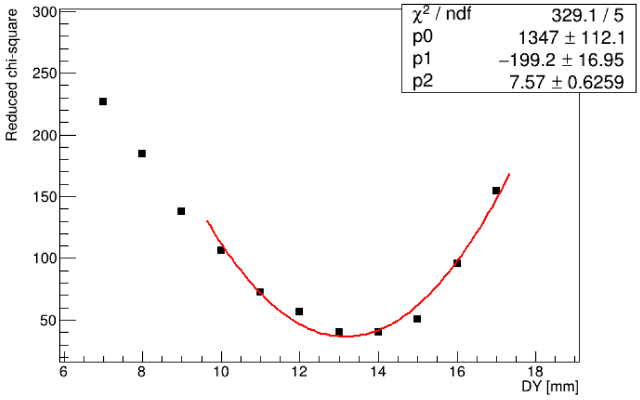

Figure 3.28: χ^2 of ^{82}Zr y_{ta} distribution for DY optimization.

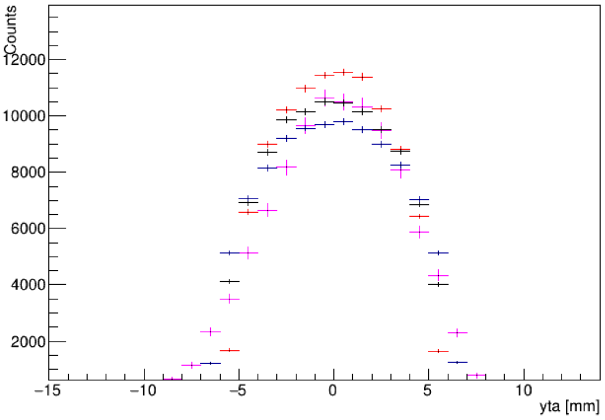

Figure 3.29: Comparison of ^{82}Zr y_{ta} reacted with target experimental distribution (purple) with different DY simulations: 11 mm (red), 12 mm (black) and 13 mm (blue).

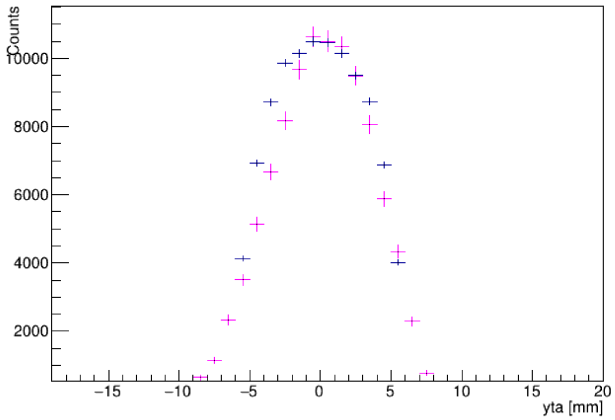

Figure 3.30: ^{82}Zr optimized y_{ta}: $DY = 12$ mm; simulation (blue) and data (purple). From a direct comparison this is the best one distribution instead of $DY = 13$ mm as suggested by χ^2.

a_{ta} distributions

The dispersive angle distribution a_{ta} is not reproduced by the simulation since there are some unknown physical parameters, necessary to describe this type of process, which are not considered. The real a_{ta} distribution is wider respect to the simulated one.

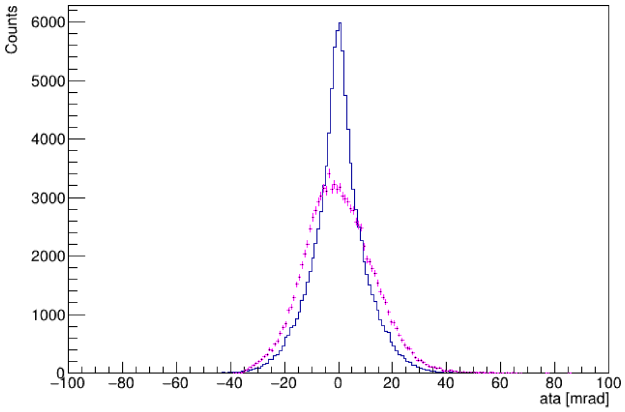

Figure 3.31: ^{84}Zr a_{ta} comparison with optimized reaction parameters: simulation (blue) and data (purple).

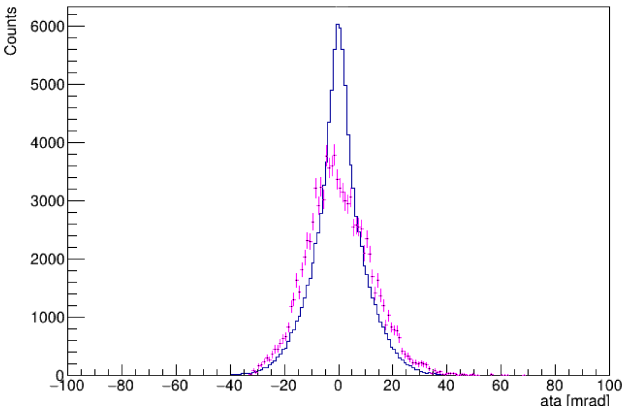

Figure 3.32: ^{82}Zr a_{ta} comparison with optimized reaction parameters: simulation (blue) and data (purple).

3.3 γ-ray Spectra Simulations

The optimal values derived from the previous analysis are necessary to reproduce γ-ray spectra. However, before doing it, there are also other important parameters that have to be properly set:

- **Transition energies**: Different decays can be distinguished by their transition energies. These experimental values are available on NNDC site [23]. In the simulation macro it is necessary to specify also the initial excited state of the transition, for this reason level schemes are fundamental for the comprehension of the observed spectra.
- **Lifetimes**: This parameter affects peak lineshape as described in Section 1.2.1 (Fig. 1.5). If the lifetime is too short a relevant fraction of the decays occurs within the target producing a tail on the left side of the peak due to a not correct Doppler correction. The excited states lifetimes used in simulations derive from literature or from considerations about peak shapes.
- **Population of excited states**: It is directly connected to the relative transition intensity and it has been calculated from experimental peak integral. Using GRETINA's Efficiency curve (Fig. 3.33) it is therefore possible to obtain the intensity of a decay using the following formula:

$$Intensity = \frac{Area}{Efficiency}$$

  Typically this method has big uncertainties due to the difficulty of a correct estimation of peak area (see spectra in Fig. 3.37 and 3.41): relative intensities are adjusted through the simulations in order to reproduce experimental spectra.

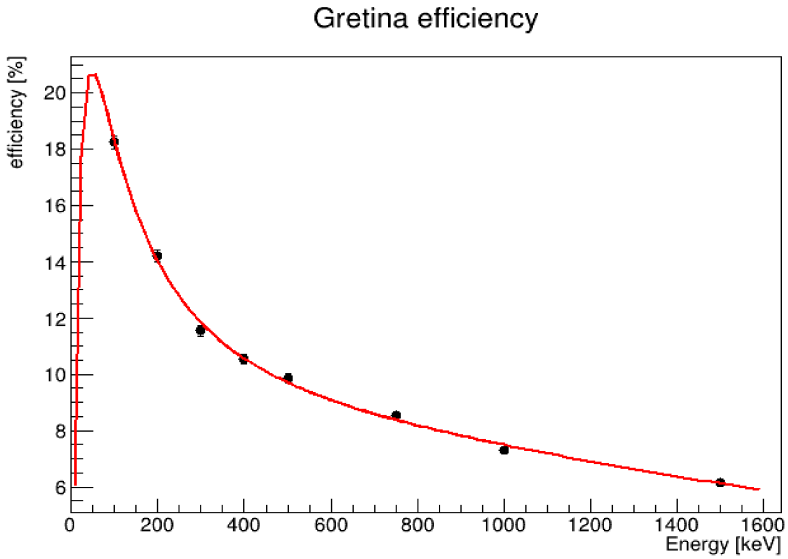

Figure 3.33: Gretina absolute efficiency. This curve has been obtained by using a calibration source of ^{152}Eu with a known efficiency fit function.

- β: Doppler correction can be simulated inserting in the macro file the information about outgoing beam velocity (Fig. 3.35 and 3.39).

Another important parameter that has to be considered in the simulation is the energy resolution which is the full width at half maximum of γ-ray peaks. A good simulation is capable to correctly reproduce not only the intensity but also the width of the peaks: this value becomes useful to verify the correctness of the simulation parameters. Typically the relative resolution of GRETINA, defined as $R = \frac{\Delta E}{E}$, is in the range [1.5% , 2%] (ΔE is the FWHM of a peak with an energy equal to E). The final results are summarized in the next two sections. Their scope is to qualitatively reproduce the experimental γ-ray spectra of ^{84}Zr and ^{82}Zr: for this reason all uncertainties are omitted.

3.3.1 ^{84}Zr Simulated Spectrum

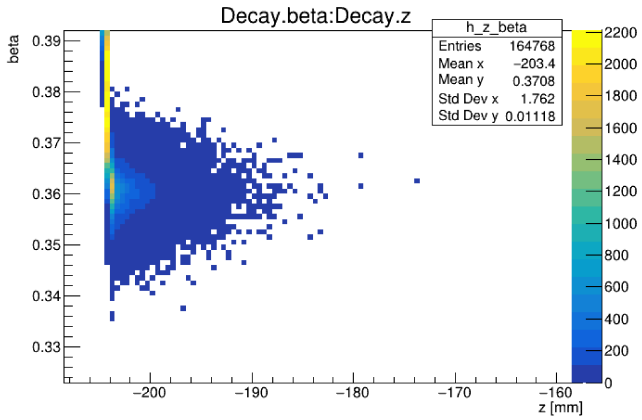

Figure 3.34: ^{84}Zr outgoing β vs. γ-decay position (z).

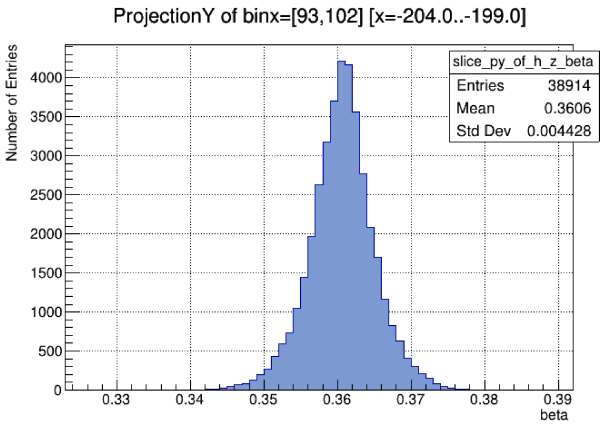

Figure 3.35: ^{84}Zr outgoing β distribution after the target. The centroid is $\beta = 0.362$.

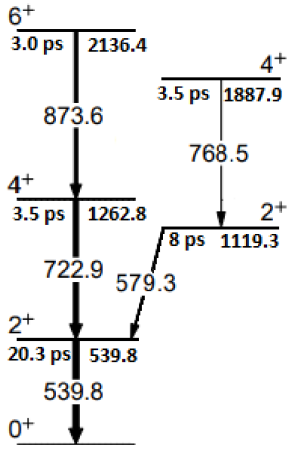

Figure 3.36: ^{84}Zr level scheme of observed low-energy states.

Energy [keV]	Lifetime [ps]	Efficiency [%]	Relative intensity [%]
539.8	20.3	9.4	50
579.3	8	9.2	1
722.9	3.5	8.5	18
768.5	3.5	8.3	14
873.6	3.0	7.9	17

Table 3.1: Parameters used as input for the simulation of ^{84}Zr spectrum.

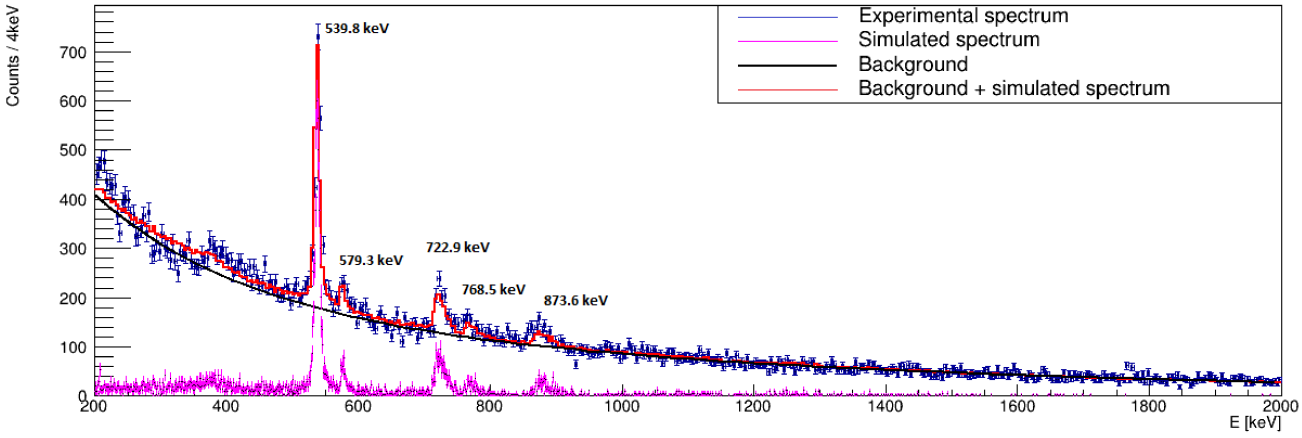

Figure 3.37: ^{84}Zr simulated spectrum overlapped to the experimental one.

In the range of [300 keV, 400 keV] the simulation is not capable to completely reproduce the background. Part of it indeed is composed by the annihilation of the positrons produced by pair production of γ-rays inside the detector. The Doppler correction algorithm tries to correct the typical 511 keV peak energy revealed considering the detecting angle of the incident photon (using the Eq. 1.4): the effect is a deviation from the exponential background shifted to the low-energy side.

3.3.2 ^{82}Zr Simulated Spectrum

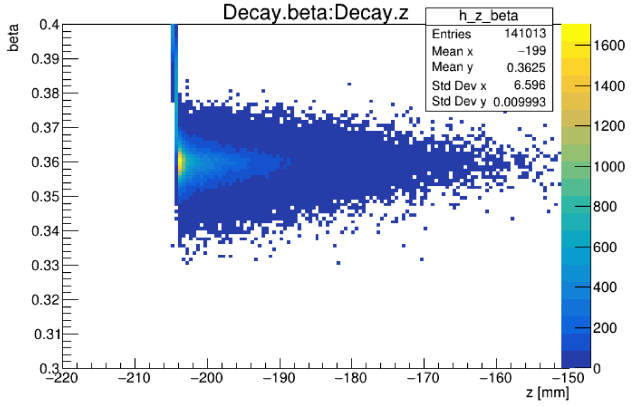

Figure 3.38: ^{82}Zr outgoing β vs. γ-decay position (z).

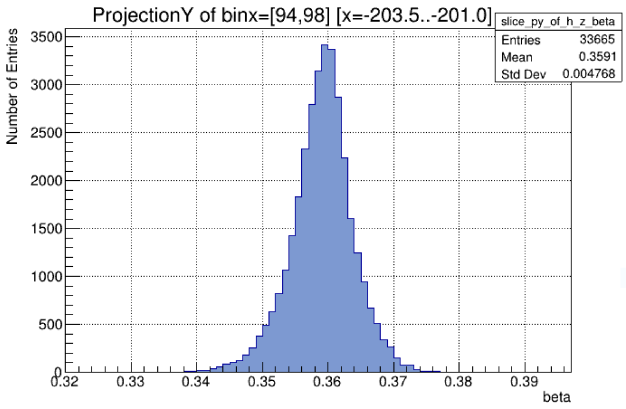

Figure 3.39: ^{82}Zr outgoing β distribution after the target. The centroid is $\beta = 0.358$.

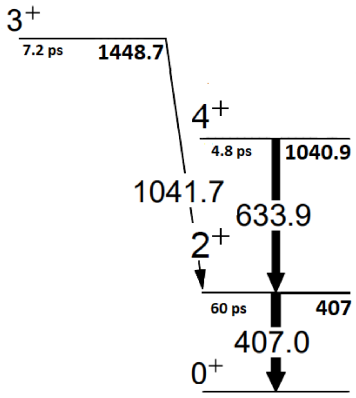

Figure 3.40: ^{82}Zr level scheme of observed low-energy states.

Energy [keV]	Lifetime [ps]	Efficiency [%]	Relative intensity [%]
407	60	10.5	50
633.9	4.8	8.9	26
1041.7	7.2	7.4	24

Table 3.2: Parameters used as input for the simulation of ^{82}Zr spectrum.

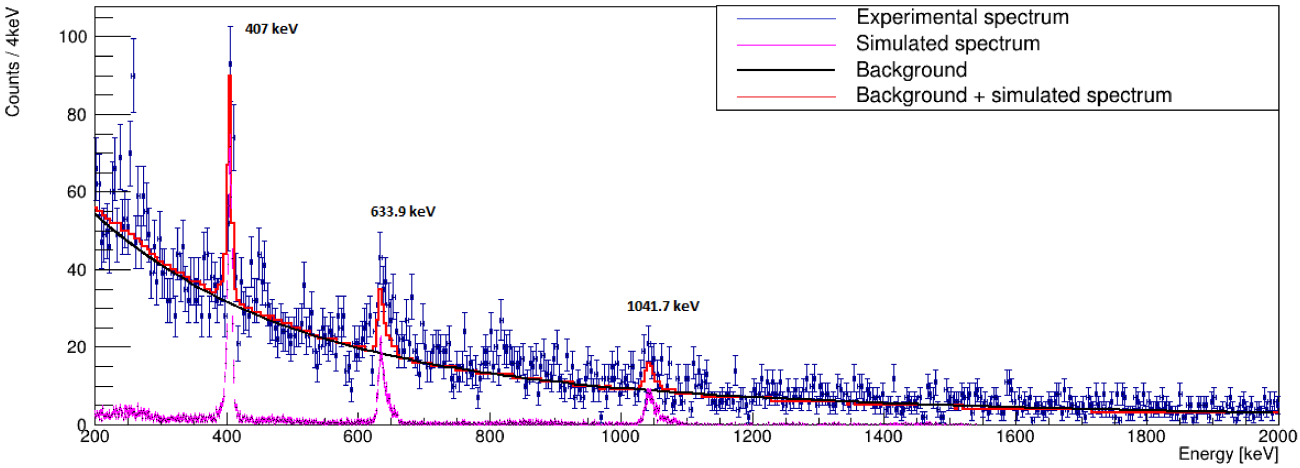

Figure 3.41: ^{82}Zr simulated spectrum overlapped to the experimental one.

This spectrum has a lower statistics and larger uncertainties respect to ^{84}Zr. There are three peaks which are not fitted by the simulation around 250 keV, 450 keV and 820 keV: they are not ^{82}Zr decays but contaminant peaks from other similar reaction channels such as ^{82}Sr and ^{82}Y.

Conclusions and Perspectives

Monte Carlo simulations play a key role in nuclear physics due to their flexibility and possibility to reproduce very complex interactions of radiation with matter, from beam interaction with a target to γ-ray spectrum. GEANT4 simulation toolkit has been successfully used to reproduce the experimental results.

Contemporary nuclear physics explores the limit of nuclear binding and the structure of radioactive isotopes far from the stability valley. The synthesis of these isotopes requires to use intermediate to high energy beams (100 AMeV to 2 AGeV) and a complex detection system for the identification of the isotopes recoiling at relativistic energies. In order to extract reliable measurement of relevant physical quantities there is the need for a realistic model that accounts for the kinematics of the beam, the nuclear recoil and the response function of the detectors in use. The complexity of the apparatus, with many free parameters, suggests using Monte Carlo simulations. Some of the parameters can be directly extrapolated from the experimental data, as done for the incoming beam momentum distribution, others, instead, are predicted from physical models, such as the knockout reactions.

This work focused on ^{84}Zr which was produced with similar beam properties to ^{86}Mo and their products, ^{82}Zr and ^{84}Mo respectively, are obtained from a similar two-neutron knockout reaction. Therefore the optimization results derived from zirconium (easier and more meaningful to analyze since it has larger statistics) can be compared with molybdenum. Through a similar procedure to that described in this work it is possible to optimize ^{84}Mo reaction parameters.

The next step in the analysis is the study of plunger setup adding the degrader information in the simulation. In this case there are three remarkable regions: before the target, between target and degrader and after the degrader. It will be necessary to find the correct value of the secondary outgoing beam energy, the corresponding degrader scale-density and the optimal reaction parameters as was done in this thesis for the first run of the experiment. Eventually, after setting all the physical information, there will be only one variable, the lifetime of the first 2^+ state of ^{84}Mo, which will be optimized comparing the simulated spectrum with the experimental one.

Bibliography

[1] A. P. Zuker, A. Poves, F. Nowacki and S. M. Lenzi. *Nilsson-SU3 self-consistency in heavy Z = N nuclei*. Physical Review Letters, 024320 (2015).

[2] R. D. O. Llewellyn et al. *Establishing the Maximum Collectivity in Highly Deformed N = Z Nuclei*. Physical Review Letters, 152501 (2020).

[3] P. Adrich et al. *A simulation tool for Recoil Distance Method lifetime measurements at NSCL*. Nuclear Instruments and Methods in Physics Research. Sect. A 598, 454-464 (2009).

[4] R. D. O. Llewellyn. *Structure and Collectivity of Highly Deformed Nuclei Along the N = Z Line*. Doctor of Philosophy, University of York (2020).

[5] C. S. Morse. *Nuclear structure of proton-rich intermediate mass nuclei studied with advanced lifetime measurement techniques*. Doctor of Philosophy, Michigan State University (2015).

[6] D. J. Morrissey et al. *Commissioning the A1900 projectile fragment separator*. Nuclear Instruments and Methods in Physics Research. Sect. B 204, 90-96 (2003).

[7] A. Stolz et al. *Production of rare isotope beams with the NSCL fragment separator*. Nuclear Instruments and Methods in Physics Research. Sect. B 241, 858-861 (2005).

[8] D. Bazin, A. Caggiano, M. Sherrill, J. Yurkon and A. Zeller. *The S800 spectrograph*. Nuclear Instruments and Methods in Physics Research. Sect. B 204, 629-633 (2003).

[9] T. Lauritsen et al. *Characterization of a gamma-ray tracking array: A comparison of GRETINA and Gammasphere using a ^{60}Co source*. Nuclear Instruments and Methods in Physics Research. Sect. A 836, 45-56 (2016).

[10] O. Klein and Y. Nishina. *Über die Streuung von Strahlung durch freie Elektronen nach der neuen relativistischen Quantendynamik von Dirac*. Zeitschrift für Physik (1929).

[11] S. Paschalis et al. *The performance of the Gamma-Ray Energy Tracking In-beam Nuclear Array GRETINA*. Nuclear Instruments and Methods in Physics Research, Sec. A 709, 44-55 (2013).

[12] *NSCL PAC 43 PROPOSAL ELEMENTS. Description of Experiment* (2019).

[13] S. Heil. *Electromagnetic Properties of ^{21}O and the Self-Calibration of Compton Tracking Arrays*. Doctor of Philosophy, University of Darmstadt (2019).

[14] H. Iwasaki et al. *Evolution of Collectivity in ^{72}Kr: Evidence for Rapid Shape Transition*. Physical Review Letters, 142502 (2014).

[15] S. A. Milne. *Investigation of Isospin Symmetry Breaking in the $f_{7/2}$ Region, Studied through One-nucleon Knockout and Lifetime Measurements*. Doctor of Philosophy, University of York (2016).

[16] H. Tokieda et al. *Performance of Focal-Plane Tracking Detector CRDC for SHARAQ*. American Physical Society, 3rd Joint Meeting of the APS Division of Nuclear Physics and the Physical Society of Japan, (2009).

[17] G. F. Knoll. *Radiation Detection and Measurement, 4th ed.*. John Wiley and Sons, Inc. (2010).

[18] K. Wang et al. *Plastic Scintillation Detectors for Time-of-Flight Mass Measurements*. Nuclear Instruments and Methods in Physics Research. Sect. A 974, 164199 (2020).

[19] J. Yurkon et al. *Focal plane detector for the S800 high-resolution spectrometer*. Nuclear Instruments and Methods in Physics Research, Sec. A 422, 291-295 (1999).

[20] S800 Documentation, `https://wikihost.nscl.msu.edu/S800Doc/`. [Online; accessed 21-October-2019].

[21] D. Bazin, O. Tarasov, M. Lewitowicz and O. Sorlin. *The program LISE: a simulation of fragment separators*. Nuclear Instruments and Methods in Physics Research. Sect. A 482, 307-327 (2001).

[22] GEANT4 website: `https://geant4.web.cern.ch/node/1`.

[23] A. Sonzogni. *National Nuclear Data Center (NNDC)*. Brookhaven National Laboratory website: `https://www.nndc.bnl.gov/nudat2/chartNuc.jsp`.